buildings

MDPI

Article

Assessment of the Density Loss in Anobiid Infested Pine Using *X*-ray Micro-Computed Tomography

João Parracha [1,2], Manuel Pereira [3], António Maurício [3], Paulina Faria [2,4], Daniel F. Lima [5], Marina Tenório [5] and Lina Nunes [1,6,*]

1 Department of Structures, National Laboratory for Civil Engineering, 1700-066 Lisbon, Portugal; jparracha@lnec.pt
2 CERIS, Instituto Superior Técnico, University of Lisbon, 1049-001 Lisbon, Portugal; mpr@fct.unl.pt
3 CERENA, Instituto Superior Técnico, University of Lisbon, 1049-001 Lisbon, Portugal; mfcp@ist.utl.pt (M.P.); pcd2045@tecnico.ulisboa.pt (A.M.)
4 School of Science and Technology, NOVA University of Lisbon, 2829-516 Caparica, Portugal
5 ISISE, Campus de Azurém, University of Minho, 4800-058 Guimarães, Portugal; daniel.asmf.lima@gmail.com (D.F.L.); tenorio.mcu@gmail.com (M.T.)
6 cE3c, Azorean Biodiversity Group, University of Azores, 9700-042 Azores, Portugal
* Correspondence: linanunes@lnec.pt

Abstract: The present study aims at evaluating the impact of anobiid damage on pine timber elements. Anobiid attack produces a diffuse damage of the elements with a set of tunnels in random directions and sizes, thus confusing quantification. Therefore, a method was developed based on *X*-ray micro-computed tomography (μ-XCT) to obtain, for naturally infested timber samples, an empirical correlation between lost material percentage (consumed by beetles) and timber apparent density (original, before degradation—OTD and residual, after degradation—RTD). The quantified density loss can then be used in further assessment of the structure. The results of the tests performed showed high correlation between original apparent density and lost material percentage (r^2 = 0.60) and between residual apparent density and lost material percentage (r^2 = 0.83), which confirms μ-XCT as a valuable tool to the required quantification. The loss of density results can be further applied on the definition of an assessment method for the evaluation of the residual strength of anobiids infested timber, thus contributing to reducing unnecessary replacement. The optimized procedure of the μ-XCT study for infested Maritime pine (*Pinus pinaster*) is presented and discussed in this article.

Keywords: wood; anobiid infestation; three-dimensional reconstruction; residual apparent density; damage assessment

Citation: Parracha, J.; Pereira, M.; Maurício, A.; Faria, P.; Lima, D.F.; Tenório, M.; Nunes, L. Assessment of the Density Loss in Anobiid Infested Pine Using *X*-ray Micro-Computed Tomography. *Buildings* **2021**, *11*, 173. https://doi.org/10.3390/buildings11040173

Academic Editors: Jorge Manuel Branco, Hélder Sousa and Elisa Poletti

Received: 7 March 2021
Accepted: 14 April 2021
Published: 17 April 2021

1. Introduction

Building materials like stone, earth or wood have been used for millennia. Wood, in particular, has played a very important role in the history of construction with its distinct physical and mechanical characteristics. However, due to its biological origin, it is susceptible to biodeterioration. Wood-decaying fungi and subterranean termites are widely regarded as the most destructive agents of timber *in usu* [1,2], though wood boring beetles like several species of the anobiid family (Coleoptera: Anobiidae) have also to be taken into consideration.

The deterioration problems are mainly limited to the sapwood [3] and are a result from the extensive network of galleries, consequent of the anobiids' wood consumption at the larvae stage. On the surface of timber, the damage tends to be only detected either by the occasional presence of frass or exit holes left by the adult beetles when emerging [4].

The older the structure, the higher the probability of timber having suffered some anobiid infestation during its service life, and thus there is a need for regular inspection

and maintenance. A correct structural safety assessment of a timber structure must include the identification of the deterioration agents and the level of degradation. When anobiid damage is found, the assessment of the remaining timber structural soundness is far from easy [5]. The diagnosis tends to be done by visual assessment of exit holes on the surface of the timber elements (e.g., [6–8]) and replacement maybe often chosen as retrofitting solution with obvious costs both for the owner and for the environment [6,9]. However, non-destructive tests (NDTs) or semi-destructive tests (SDTs) can also be used for the vulnerability assessment of timber structural elements. Some examples are the drilling resistance, hardness, and *X*-ray radioscopy tests, and both NDTs and SDTs are used for the evaluation of timber density, biological defects, and voids [10–12]. Moreover, NIR spectroscopy can be applied for the evaluation of timber decay [13], whereas stress waves, ultrasound methods, and active thermography tests can be used for the detection of voids [14–16].

If a decision to keep the infested structural element is reached to account for the insects' damage, a very conservative approach is typically followed where a significantly reduced cross section or reduced mechanical properties for the original cross sections are assumed [7,9] even though the exact level of deterioration is, in fact, not known.

The visual assessment of degraded timber elements is not completely representative since the estimated internal holes volume grade (%) tends to be much greater than the visually estimated voids' surface grades [6,8]. This highlights the importance of knowing the percentage of real loss of material (wood consumed by anobiids) as well as the loss of density. This will allow to conclude on the structural safety, as the knowledge of timber's original (before anobiids' degradation) and residual (after anobiids' degradation) apparent densities is fundamental to assess timber soundness as these parameters are highly correlated with the relevant mechanical characteristics.

In this sense, *X*-ray micro-computed tomography (µ-XCT) may be used to visualize and quantify a three-dimensional structure. It uses the same principles of medical computed tomography (CT) with the difference that allows' seeing micrometric 3D details in very small samples [17]. However, it is not possible yet to use µ-XCT for in situ observations and small-size samples need to be collected from the structural elements to be submitted to µ-XCT in the laboratory [18]. In addition, µ-XCT has micrometric scale range resolution, which enables higher accuracy in 3D volume visualization and measurements [19].

The use of CT or µ-XCT has been increasing in recent years, namely for the study of deterioration patterns of different materials. Examples are the detection of insect damage on wood (i.e., [20–22]) or bamboo [23] and also the quantification of galleries built by shipworms on wood applied in marine environment [24].

Fuchs et al. [20] used CT to observe the nest gallery of the drywood termite *Cryptotermes secundus* in order to contribute to termite management by determining wood consumption rates of termite colonies. Himmi et al. [21] analyzed the nesting biology of the drywood termite *Incisitermes minor* using CT images, whereas Watanabe et al. [23] used *X*-ray-CT for the evaluation of the larval growth process and bamboo consumption by the beetle *Dinoderus minutus*. These latter authors observed that each larva produced a tunnel length of 0.98 mm and a bored volume of 1.06 mm^3 per day.

This paper aims at evaluating the impact of anobiid damage on pine timber elements. A method was developed based on *X*-ray micro-computed tomography (µ-XCT) to obtain, for naturally infested timber samples, an empirical correlation between lost material percentage (consumed by beetles) and timber apparent density (original, before degradation and residual, after degradation). The loss of density values were then applied on the definition of an initial approach for an on-site assessment of infested timber structural elements [5]. This paper presents and discusses the diverse steps needed during the µ-XCT study, intending to improve the efficiency and scope of the technique for the study of wood.

2. Materials and Methods

2.1. X-Ray Micro-Computed Tomography Study

In this study, μ-XCT was used as a 3D microscopy technique to assess the anobiids galleries (visualizing its spatial distribution and morphology) and calculate the volume of the voids, and therefore the amount of lost material (consumed by anobiids).

The usual procedure applied to all μ-XCT scanning processes was also applied in the present study and consists of the following major steps (Figure 1) that are further described below in Sections 2.2–2.5.

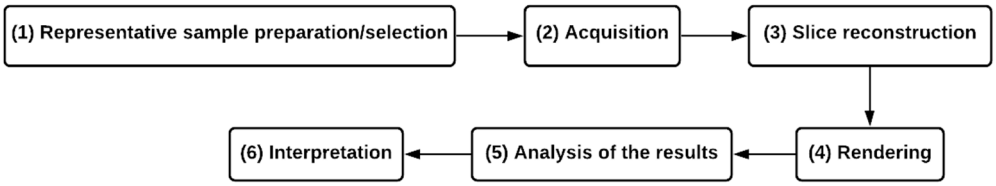

Figure 1. Scheme of the usual procedure applied to all *X*-ray micro-computed tomography (μ-XCT) scanning processes.

2.2. Representative Sample Preparation/Selection

A maritime pine (*Pinus pinaster* Ait.) roof beam was collected from a residential building in Lisbon, Portugal after about 60 years of service life. The presence of different levels of anobiid infestation was easily recognized on the sapwood. The main insect responsible for the deterioration was identified as *Nicobium castaneum* Olivier by the size of the galleries, the characteristics of the frass, and of the several cocoons that were retrieved from the samples.

After the insect identification, timber was divided in 4 segments (3 containing degradation and the sound heartwood) and cut to produce approximately 40 × 20 × 40 mm^3 samples. These samples were then crosscut to obtain 17 "new" paired samples, with approximately 40 × 20 × 10 mm^3, that were adequate for μ-XCT [5]. These samples (Figure 2) representing the varying degrees of degradation along the beam were submitted to μ-XCT. The heartwood was not used.

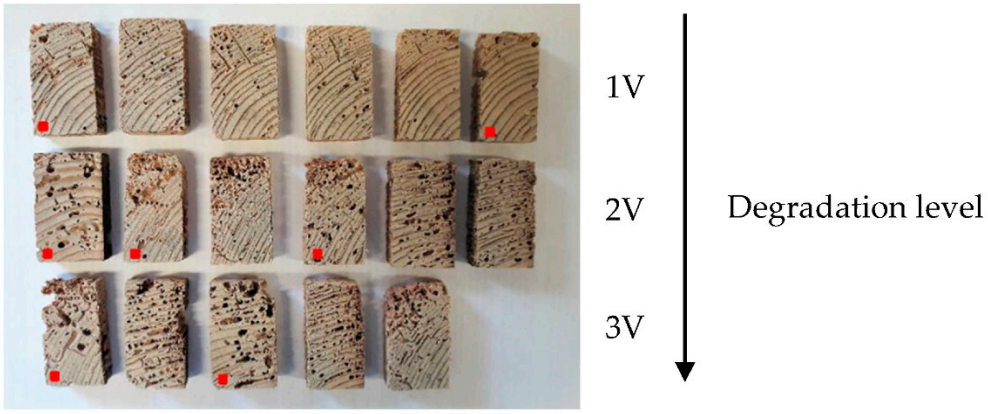

Figure 2. Sample preparation: 17 varying degrees of infested samples to be analyzed in μ-XCT were visually divided into 3 levels of degradation (all samples that were redistributed to a different level after μ-XCT results are marked in red). Average size of samples = 40 × 20 × 10 mm^3.

The samples were assigned into 3 levels of degradation (level 1V, 2V, and 3V) through a visual analysis of the deterioration and considering the area of the emergence holes at the exposed surfaces of the degraded samples (Figure 2). Level 1V corresponds to the lowest degradation level and level 3V to the highest. It should be noted that this visual grading approach had already been proved as not fully representative of the internal degradation [7,8]. After determining the tomographic parameters of interest (wood and

voids' volume), the designation levels of the samples were readjusted according to the results of the lost material percentage.

Before the scanning procedure, all samples were conditioned for 2 weeks in a climatic chamber (temperature (T) of 20 ± 2 °C and a relative humidity (RH) of 65 ± 5%) to stabilize and reach maritime pine sapwood' reference moisture content (12%) [25]. No previous treatment was required for the samples to be submitted to µ-XCT as this technique requires very little sample preparation and, regularly, a sample can be scanned exactly as provided; however, the best sample size required for the scanning procedure has to be taken into consideration [26].

2.3. Scanning Procedure (Acquisition)

All maritime pine samples were scanned with a compact desktop with micrometric range resolution, µ-XCT Skyscan 1172 microtomograph (Bruker Instruments, Inc., Billerica, MA, USA), using computer-controlled tomography acquisition, processing, reconstruction, and analysis software packages (CTAn and ImageJ software provided by Bruker (Billerica, MA, USA) and NIH (Bethesda, MD, USA), respectively).

However, prior to each sample scanning procedure, a decision must be made concerning the best sample size, which is determined based on at least the following criteria: the aim of the problem to be studied and the physical, the geometrical, and operating constraints of the scanner. The next step in the preparation for scanning procedure of the µ-XCT methodology is choosing optimal scanner settings. There is a wide range of scan settings that substantially affect image quality such as resolution, scanner voltage, scan time, number of images acquired, angle of rotation, etc.

Resolution selection may be the first major factor that affects a µ-XCT scan. A resolution about 1000 times smaller than the width of the sample is recommended; however, reference standards exist and may be used [26,27]. A maximum resolution of 2 µm was used in the present study (Table 1), although, a generally accepted standard for industrial CT systems does not exist yet. *X*-ray scanner voltage is highly dependent on the type of material studied and their composition. For biological samples, a voltage in a range of 30 to 100 kV is recommended [26].

Table 1. Summary of the parameters used in the scanning procedure.

Parameters			
Maximum resolution	2 µm	Voltage	60 kV
Filament current	165 µA	Number of images	288
Angle of rotation	0.7°	Filters	Al 0.5 mm
Voxel Size	18.09 µm	File type	16-bit

The scanning time used for each sample was 1.5 h. Scanning time varies according to the system used, for example, due to the detector sensitivity or to the distance from source to detector [28], while the number of images required varies with the sample size. Furthermore, in our case, the need to obtain the most information from each scan suggests considering at least an oversize and multi-acquisition setting as a constraint. Therefore, a larger sample could require a longer time of acquisition if multiple scans were performed. Moreover, large samples have magnification limitations due to conic beam configuration. A reduction in the angle of rotation as well as an increase in the number of images acquired will, naturally, lead to a production of images of better quality. However, the benefit level may not be justificatory because such option will contribute to increasing scan time, reconstruction time, and data size [29]. At the end, the best settings solution for each scanning step should be found considering the output parameters that were previously defined.

During the scanning process, the studied sample must be fixed on a support while rotating in steps around a fixed vertical axis [30]. A shadow projection image at each angular position is taken and 2D digital radiography images sets are obtained. Later,

through reconstruction and rendered processes, using Skyscan-Bruker software, a set of 2D reconstructed object slice images can be combined/rendered to produce a virtual 3D reconstructed object model.

A summary of the parameters used in the scanning procedure are presented in Table 1. Besides these parameters, the distance between the *X*-ray source and the sample, as well as the distance between the *X*-ray source and the detector was 257 and 350 mm, respectively. The scanning time was 1.5 h and a 0.5 mm aluminium filter was used for absorbing the low-energy *X*-rays, thereby reducing noise.

The parameters presented in Table 1 were applied in the scanning procedure of all studied samples. After the selection of the shape and the size of samples, the *X*-ray microtomography operation procedure was optimized to produce the best possible images [30–34].

2.4. Reconstruction

Reconstruction process follows the scanning procedure, and here the 3D volume is reconstructed from the 2D digital radiography image stacks that were previously acquired. For the reconstruction process, the NRecon software, provided by Bruker, was used. This software allows the adjustment of three reconstruction parameters: smoothing, beam-hardening factor, and ring artefact reduction. These parameters will obviously affect the quality of the acquired 3D object. However, there are no generalized universal optimal parameters, and the best solution for each case study depends on the type of scanner used as well as the type of material studied. It is also possible to choose the type of output file: 16-bit or 32-bit. Though both options are valid, the set of images exported in a 32-bit file has the best quality. The area to be reconstructed also needs to be selected and should correspond to the area of interest. To save time and to have a manageable size of the data sets, some less relevant areas should not be considered [29], and a slightly larger area than that required should be reconstructed, as this ensures that critical data are retained.

Table 2 shows the reconstruction parameters used in this study. These parameters were used for the reconstruction of all studied replicates. The data was exported to 32-bit files.

Table 2. Reconstruction parameters adopted using NRecon software.

Parameter	Description	Suggested Setting
Smoothing	Smooth images and removes noise	Width; 3 pixels
Beam-hardening factor correction	Correct for the absorption of lower-energy *X*-ray on the outside of the specimen	30–55%
Ring artefact reduction	Correct for the nonlinear behavior of pixels causing ring artefacts	≈20

Next, DataViewer software was used to adjust the grayscale of images to enable a better visualization (Figure 3).

It is also necessary to choose the images viewing plane that are going to be examined. There are 3 possible options (3D objects): coronal images (radial plane)—axis xy; sagittal images (tangential plane)—axis xz; trans axial images (transverse plane)—axis yz. In this study, the coronal plan was chosen because it was the plan where the images had less visible artefacts and, because of that, it was easier to distinguish between wood and voids (tunnels formed by beetles).

With the acquisition of the 3D object, it is now possible to visualize it using a visualization program (e.g., CTVox software, provided by Bruker). The reconstructed 3D object was visualized using CTVox software (Figure 4).

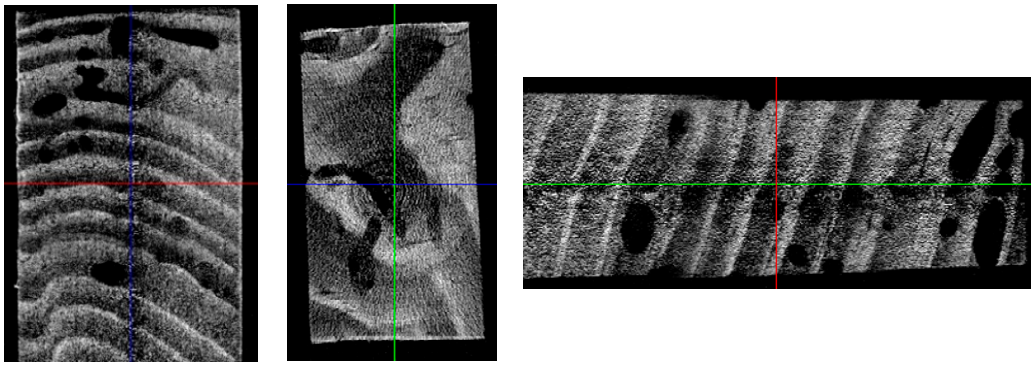

(**a**) (**b**) (**c**)

Figure 3. Two-dimensional images of the reconstructed object (samples approximately 40 × 20 × 10 mm^3): (**a**) xy: coronal plane; (**b**) xz: sagittal plane; (**c**) yz: trans axial plane.

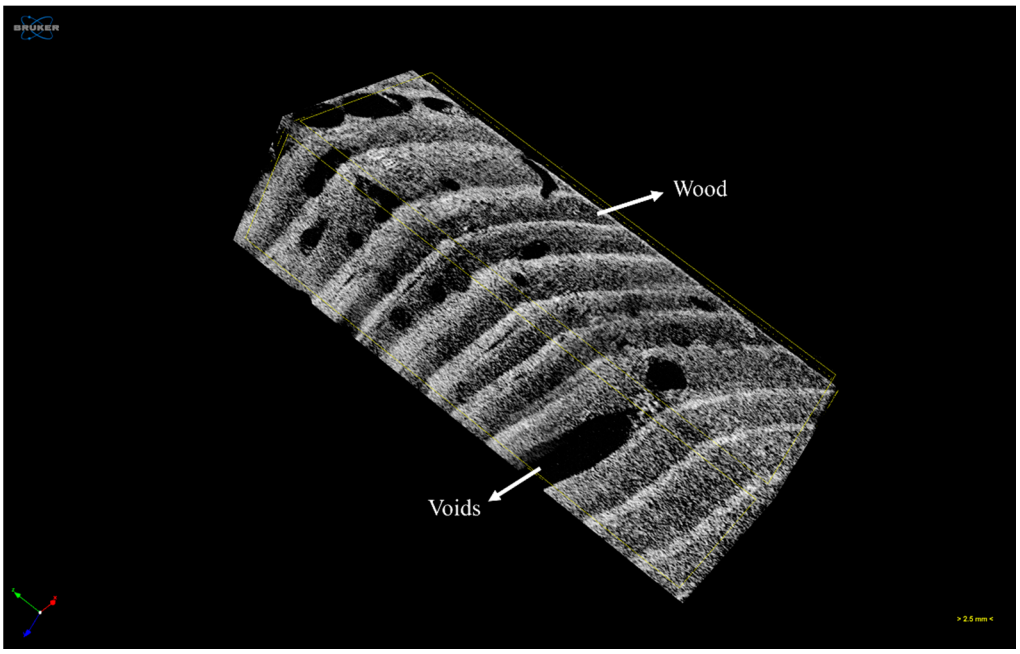

Figure 4. Reconstructed 3D object. Visualization using CTVox software.

2.5. Analysis

After the reconstruction procedure, the images can be analyzed and parametrized to obtain quantitative information (the values of the parameters of interest). This process is highly dependent on the software used. For this study, CTAn software, provided by Bruker, was used together with ImageJ software (https://imagej.nih.gov/ij/, accessed on 13 April 2021), provided by NIH, for image processing and calculation. In this case study, ImageJ software allows complementarity with CTAn, enabling easier and more flexible definition of regions of interest (ROI) in image stacks and an auto interpolation of a subset of images, which can bring some advantages linked to the elimination of local noise in stacks and sub stacks of tomographic slices, for instance. In this case study, the segmentation step is one of the most important imaging treatments that is made in this phase and consists in validly transforming the original images, in a scale of 256 gray levels, into simpler binary images (Figure 5). With these images, it is now possible to separate the features of interest (wood and voids). These features must be separated as good as possible for the calculation process. Note that those images continue to have noise, and it is impossible to remove it completely during the entire μ-XCT process. For this reason,

this step must be carried out with special attention and by a single user, so that the study is not misrepresented, mistaking, for example, wood (e.g., early growth) with voids or voids with noise. It is very important to remove the noise while keeping the structural and morphological information, that may be at the same order of scale as the noise [35]. The accuracy of the estimated parameters' values is strongly dependent on the quality and robustness of segmentation process [36]. A generalized image processing algorithm must be defined (Table 3) to segment three-dimensional images of complex materials to extract the different phases (in this study, there are 2 phases: wood and voids).

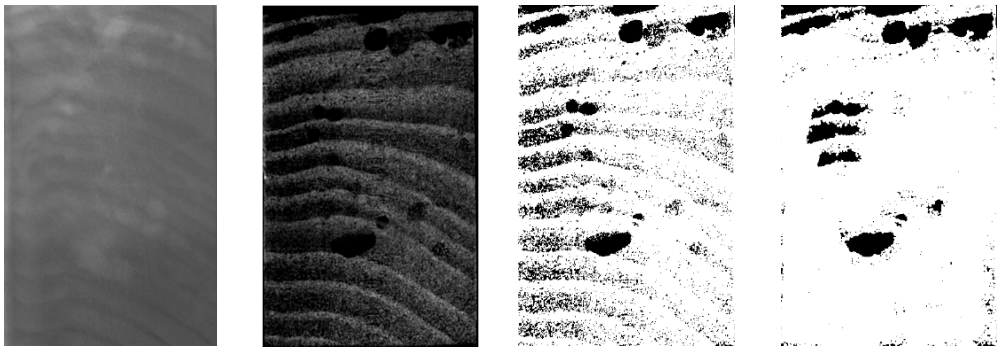

Figure 5. Images of the various steps related with μ-XCT methodology: (**a**) scanning procedure; (**b**) after reconstruction process; (**c**) analysis—binary image; (**d**) binary treated image ready for calculation.

Table 3. Image processing algorithm used to segment 3D images.

Parameter	Description	Suggested Setting
Thresholding	Segments the foreground from background to binary images	Global; low level 17, high level 255
Despeckle	Removes speckles from binary images	Remove white speckles <500 voxels; remove black speckles <150 voxels
Morphological operations	Fills the holes and closes the pores	2D space: Closing; Kernel round, radius 5

The area to be analyzed from the reconstructed images, i.e., region of interest (ROI), must be selected using a free-hand tool. Then, an auto interpolation among different ROI levels will produce the total volume of interest (VOI) for all selected frames.

Thresholding is one of the first and most important parameters to be selected. Threshold converts the set of images, originally in a grayscale, in a binary set. From the application of this parameter, sets of binary discrete images are established, with the two structural parameters of interest defined and separated. However, the choice of threshold can vary from user to user, and therefore result in differences that are larger than the experimental differences themselves [36]. Due to that fact, global thresholds must be chosen by one user and kept during the entire study. This reinforces the importance of having a defined basis algorithm (Table 3). Before thresholds, images can and should be filtered to remove noise. Bruker's CTAn software allows the adjustment of analyzing parameters such as filter, threshold, despeckle, and additional morphological operations. Each one of these parameters has as a function of treating image sets to get a final set of images, from which interest parameters can be easily calculated.

Finally, with the images treated according to the interests of the study and with the defined volume of interest (VOI), it is possible to calculate the parameters of interest (wood and voids) values. These parameters' values are obtained through a parametric 3D analysis of the object.

The results (output parameters) are obtained as a *txt* file exported from CTAn. From the estimated output parameters values, two of them can be highlighted: *tissue volume*, referring to the volume of interest (VOI), and *bone volume*, referring to the wood itself (skeleton). As this technique has been developed to study human bones, several less obvious terms were kept even for different uses.

The *tissue volume* and the *bone volume* will correspond to that of interest defined previously, as voids volume will correspond to the difference between VOI and *bone volume*. Besides these parameters, it is also possible to extract a set of other parameters, such as the length of the tunnels inside wood, for example, that provide a more thorough object analysis. However, by using these values one must be cautious, in the sense that the used algorithm was defined for the study of two particular interest parameters (wood and voids volumes).

After the scanning procedure, all 17 samples were conditioned for 2 weeks in a climatic chamber (T = 20 ± 2 °C and RH = 65 ± 5%) to stabilize and reach a moisture content identical to that of reference (12%). After that, all the samples were weighed using a scale with a precision of 0.001 g.

Original apparent density (reference density) is calculated by Equation (1):

$$\rho_{original} = \frac{m}{o.v} \quad (1)$$

in which m is the sample weight in kg and o.v is the object volume (wood) in m^3.

Residual apparent density (after degradation) is calculated by Equation (2):

$$\rho_{residual} = \frac{m}{t.v} \quad (2)$$

in which m is the sample weight in kg and t.v is the total volume (wood and voids, corresponding to the VOI) in m^3.

3. Results and Discussion

The results of the output parameters (total volume and wood volume), lost material percentages, and sample weights are presented in Table 4.

Table 4. Output parameters, lost material percentages, and sample weights.

Degradation Level	Sample	*Total Volume*	*Wood Volume*	Lost Material	Weight
		cm^3	cm^3	%	g
Level 1	1.1	8.798	7.868	10.57	4.541
	1.2	9.250	8.339	9.85	4.776
	1.3	8.913	8.074	9.41	4.520
	1.4	9.168	8.299	9.48	4.308
	1.5	7.352	6.731	8.45	4.360
	1.6	7.576	6.293	16.94	3.455
Level 2	2.1	8.529	7.811	8.42	4.763
	2.2	7.020	5.413	22.89	2.912
	2.3	7.291	5.865	19.56	2.807
	2.4	6.319	4.854	23.18	2.152
	2.5	8.179	7.158	12.48	3.862
	2.6	7.021	6.022	14.23	2.988

Table 4. *Cont.*

Degradation Level	Sample	*Total Volume*	*Wood Volume*	Lost Material	Weight
		cm^3	cm^3	%	g
Level 3	3.1	8.774	7.071	19.41	3.412
	3.2	8.631	6.309	26.90	2.544
	3.3	7.216	6.260	13.25	3.084
	3.4	8.011	6.224	22.31	3.212
	3.5	7.154	5.595	21.79	2.782

Table 5 shows the average results of total volume, wood volume, lost material percentage, mass of the samples and densities for the initial sample distribution, based on visual survey.

Table 5. Initial sample distribution. Average values and relative standard deviations for the output parameters, mass, density, and loss of density.

Degradation Level		1V	2V	3V
Number of samples		6	6	5
Volume (cm^3)	Total	8.452	7.393	7.957
	Wood	7.601	6.187	6.292
Lost material (%)		10.78 ± 3.52	16.79 ± 5.49	20.73 ± 4.87
Weight (g)		4.327	3.247	3.007
Densities (kg/m^3)	Original	571 ± 65	518 ± 83	481 ± 44
	Residual	510 ± 45	433 ± 64	380 ± 36
	Loss	10.7 ± 2.89	16.4 ± 4.68	20.9 ± 5.65

Through analysis and interpretation of Table 5, it can be considered that on average the levels of degradation proposed in Section 2.2 represent the real degradation. The level of loss of density increases with the degradation level (Table 4). Nevertheless, this tendency is not verified for all samples (Figure 2). One of the samples with the highest percentage of lost material (sample 2.2–22.89 LM%) belongs to the second "level of degradation", which would be where the existing degradation, as well as the percentage of lost material was supposed to be lower. This sample should have been placed at the highest level of degradation (level 3V). This confirms what was expected: visual assessment of timber beam samples was not accurate, and a redistribution of the samples per each level needs to be done (in Figure 2, all samples that were redistributed to a different level are marked in red). It should be noted that samples with the highest redistribution by levels are at levels 2V and 3V (5 out of 7 samples redistributed), which proves that a visual grading approach is more efficient for low levels of degradation. This time, the samples will be reordered per level according to the "real" lost material percentages (calculated through µ-XCT study). This fact also confirms that there is not a clear linear correlation between the area of emergence holes at exposed surfaces and the wood specimen's strength so that the structural soundness of anobiids colonized timber cannot be acceptably assessed through examination of the exposed surfaces [6–8].

A reorganization of the samples per level of degradation was proposed (Table 6). This time, **level 1** corresponds to <10% of lost material, **level 2** to a lost material between 10% and 20%, and **level 3** to >20% of lost material.

Table 6. Reorganized sample distribution. Average values and relative standard deviations for the output parameters, mass, density, and loss of density.

Degradation Level		1	2	3
Number of samples		5	7	5
Volume (cm^3)	Total	8.642	7.836	7.427
	Wood	7.850	6.648	5.679
Lost material (%)		9.12 ± 1.05	15.16 ± 2.45	23.54 ± 1.84
Weight (g)		4.545	3.449	2.720
Densities (kg/m^3)	Original	582 ± 74	517 ± 62	495 ± 45
	Residual	529 ± 53	439 ± 70	386 ± 28
	Loss	9.2 ± 0.64	15.3 ± 3.5	21.9 ± 1.4

Brozovsky et al. [37] also proposed the definition of 3 levels of degradation, but once again based on a cross-section reduction that was suggested based on only the examination of the exposed surfaces.

As expected, the apparent densities (original and residual) decrease with increasing lost material percentage. According to the proposed level definition, level 3 has the highest density loss, with an average value of 21.9 ± 1.4%. On the other hand, level 1 has the lowest density loss (9.2 ± 0.64%), followed by level 2, with a loss of 15.3 ± 3.5%. For all samples, an average loss of density of 80 ± 24 kg/m^3 (15.4 ± 5.5%) was obtained. In addition, the average values obtained for the original theoretical density and the residual density were 529 ± 53 kg/m^3 and 439 ± 70 kg/m^3, respectively.

Figure 6 shows the correlation between lost material percentage (LM%) and original density (OTD) and between lost material percentage (LM%) and residual density (RTD). As can be seen, a medium correlation (r^2 = 0.60) was obtained between LM% and OTD, which becomes higher (r^2 = 0.83) when comparing LM% and RTD. As expected, results confirm that the higher the density, the lower the LM%.

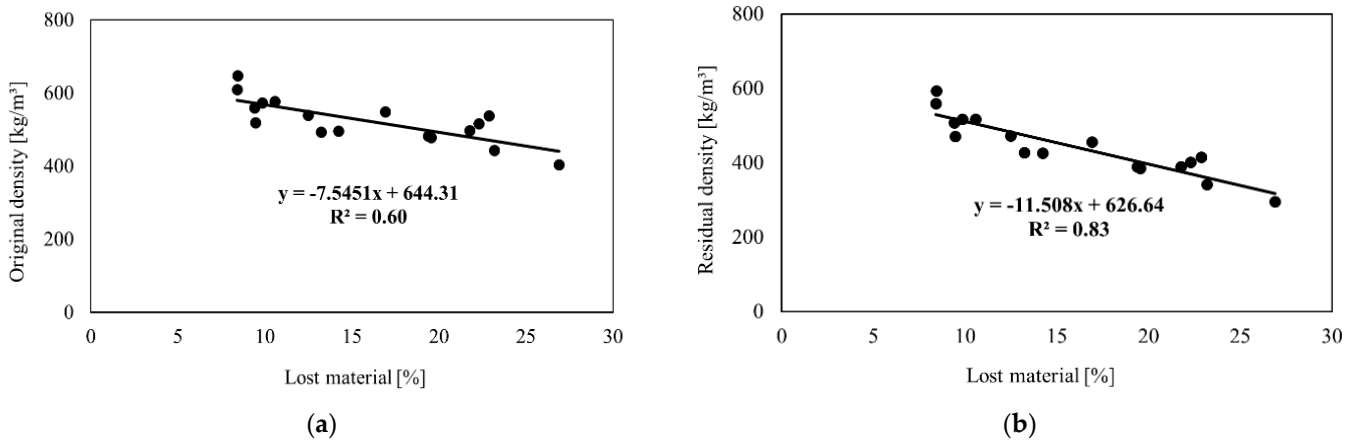

Figure 6. Correlations between lost material percentage (LM%) and timber apparent density, original (OTD) (**a**) and between LM% and timber apparent density, residual (RTD) (**b**) (adapted from [1]).

The results also suggest that timber density is a determinant parameter for the assessment of timber quality, but also confirm that the μ-XCT method was well applied in this research study.

The loss of density results (Figure 6) were then used by the same research team in the definition of an assessment method for the evaluation of the residual strength of anobiids infested timber, thus contributing to reduce unnecessary replacement. Details of this work have been reported elsewhere [5]. Indeed, the method proposed by Parracha et al. [5] included the definition of correlations between density loss values, obtained in this study

using μ-XCT methodology, and mechanical properties (screw withdrawal force and shear parallel to the grain strength). By using these correlations, the density loss of a degraded structural element can be estimated via the screw withdrawal force. Consequently, the shear strength parallel to the grain can be obtained via density loss values, thus enabling an improved quantitative assessment of the timber elements residual strength.

4. Conclusions

This research is aimed at two main objectives in order to evaluate the impact of anobiid damage on pine timber structures by: (1) establishing a valid empirical correlation among lost material percentage and the loss of density; (2) presenting μ-XCT guidelines and suggestions that can be used for the assessment of degraded timber elements.

Regarding the first objective, the results showed a medium experimental correlation among lost material percentage and original apparent density. A higher experimental correlation was obtained when comparing lost material percentage and residual apparent density. It was also concluded that visual assessment of degraded samples was not accurate, with no clear correlation among the area of emerging holes at exposed surfaces and the wood specimen's strength. Furthermore, the loss of density values calculated in this study were then used on the definition of a method for evaluating the impact of anobiid damage on timber structures [5], by establishing a valid correlation among the loss of density and the loss of mechanical properties.

Concerning the second objective, suggestions and guidelines that can be used during a μ-XCT study were provided as well as all the procedure inherent to μ-XCT methodology. The applicability of μ-XCT to define the relevant parameters for anobiid damage was confirmed being this knowledge of fundamental importance for the future validation of relevant non-destructive and semi-destructive techniques. However, μ-XCT is not a non-destructive technique, and it is not yet possible to use this technique for in situ observations. Therefore, if relevant, small size samples need to be collected from the structural elements to be submitted to μ-XCT in the laboratory.

Within the context of a broader implicit program aiming to set up better quality and/or quantitative integrated multidisciplinary research on random heterogeneous biological materials used as a heritage civil engineering and architectural material, this study is suggestive and demonstrates the applicability potential of μ-XCT methodology and technology. It enables combining qualitative 3D visualization and qualitatively and validly estimating at least some of its 3D spatial structure parameters. Therefore, it can provide new insights and guidance to more systematic and detailed investigation. This way, this study highlights integrated research for more rational design and control of wood deterioration. Further developments are on-going to optimize the micro-*X*-ray CT method applied for the study of wood deterioration caused by wood boring beetles, thus allowing not only enhancement of vulnerability assessment of timber structural elements, but also contribution to pest management by determining wood consumption rates.

Author Contributions: Conceptualization, L.N.; Data curation, J.P., M.P. and A.M.; Formal analysis, J.P.; Funding acquisition, P.F. and L.N.; Investigation, J.P., M.P., A.M., D.F.L. and M.T.; Methodology, M.P., A.M. and L.N.; Project administration, L.N.; Resources, M.P. and A.M.; Supervision, P.F. and L.N.; Validation, M.P., A.M., P.F. and L.N.; Writing—original draft, J.P.; Writing—review & editing, M.P., A.M., P.F., D.F.L., M.T. and L.N. All authors have read and agreed to the published version of the manuscript.

Funding: The authors acknowledge the support given by Portuguese Foundation for Science and Technology (FCT) within research projects: PTDC/EPH-PAT/4684/2014 (DB-HERITAGE), PTDC/ECM-EST/1072/2014 (Pro-Timber), Pest-OE/CTE/UI4028/2011 (CERENA) and UIDB/04625/2020 (CERIS).

Institutional Review Board Statement: Not applicable.

Informed Consent Statement: Not applicable.

Data Availability Statement: The data presented in this study are available on request from the corresponding author.

Conflicts of Interest: The authors declare no conflict of interest.

References

1. Parracha, J.L.; Pereira, M.F.C.; Maurício, A.; Machado, J.S.; Faria, P.; Nunes, L. It's what's inside that counts: An assessment method to measure the residual strength of anobiids infested timber using micro-computed tomography. In Proceedings of the SHATIS'2019–5th International Conference on Structural Health Assessment of Timber Structures, Guimarães, Portugal, 25–27 September 2019; p. 10.
2. Eaton, R.A.; Hale, M.D.C. *Wood: Decay, Pests and Protection*; Chapmman & Hall Ltd.: London, UK, 1993.
3. EN 350:2016. *Durability of Wood and Wood-Based Products–Testing and Classification of the Durability to Biological Agents of Wood and Wood-Based Materials*; European Committee for Standardization: Brussels, Belgium, 2016.
4. Bravery, A.F.; Berry, R.W.; Carey, J.K.; Cooper, D.E. *Recognising Wood Rot and Insects Damage in Buildings*; Building Research Establishment: Garston, UK, 1992.
5. Parracha, J.; Pereira, M.F.C.; Maurício, A.; Machado, J.S.; Faria, P.; Nunes, L. A semi-destructive assessment method to estimate the residual strength of maritime pine structural elements degraded by anobiids. *Mater. Struct.* **2019**, *52*, 1–11. [CrossRef]
6. Nunes, L.; Parracha, J.; Faria, P.; Palma, P.; Pereira, M.F.C.; Maurício, A. Towards an assessment tool of anobiid damage of pine timber structures. In Proceedings of the IABSE Symposium 2019 Guimarães "Towards a Resilient Built Environment-Risk and Asset Management", Guimarães, Portugal, 27–29 March 2019; p. 8.
7. Cruz, H.; Machado, J.S. Effects of beetle attack on the bending and compression strength properties of pine wood. *Adv. Mater. Res.* **2013**, *778*, 145–151. [CrossRef]
8. Gilfillan, J.R.; Gilbert, S.G. Development of a technique to measure the residual strength of woodworm infested timber. *Constr. Build. Mater.* **2001**, *15*, 381–388. [CrossRef]
9. Cruz, H.; Yeomans, D.; Tsakanika, E.; Macchioni, N.; Jorissen, A.; Touza, M.; Mannucci, M.; Lourenço, P.B. Guidelines for on-site assessment of historic timber structures. *Int. J. Archit. Herit.* **2015**, *9*, 277–289. [CrossRef]
10. Cuartero, J.; Cabaleiro, M.; Sousa, H.S.; Branco, J.M. Tridimensional parametric model for prediction of structural safety of existing timber roofs using laser scanner and drilling resistance tests. *Eng. Struct.* **2019**, *185*, 58–67. [CrossRef]
11. Piazza, M.; Riggio, M. Visual strength-grading and NDT of timber in traditional structures. *J. Build. Apprais.* **2008**, *3*, 267–296. [CrossRef]
12. Lechner, T.; Sandin, Y.; Kliger, R. Assessment of density in timber using X-ray equipment. *Int. J. Archit. Herit.* **2013**, *7*, 416–433. [CrossRef]
13. Kandemir-Yucel, A.; Tavukcuoglu, A.; Caner-Saltik, E.N. In situ assessment of structural timber elements of a historic building by infrared thermography and ultrasonic velocity. *Infrared Phys. Technol.* **2007**, *49*, 243–248. [CrossRef]
14. Rivera-Gómez, C.; Galán-Marín, C. In situ assessment of structural timber elements of a historic building by moisture content analyses and ultrasonic velocity tests. *Int. J. Hous. Sci.* **2013**, *37*, 33–42.
15. Kordatos, E.Z.; Exarchos, D.A.; Stavrakos, C.; Moropoulou, A.; Matikas, T.E. Infrared thermographic inspection of murals and characterization of degradation in historic monuments. *Constr. Build. Mater.* **2013**, *48*, 1261–1265. [CrossRef]
16. Feio, A.; Machado, J.S. In-situ assessment of timber structural members: Combining information from visual strength grading and NDT/SDT methods–A review. *Constr. Build. Mater.* **2015**, *101*, 1157–1165. [CrossRef]
17. Baird, E.; Taylor, G. X-ray micro-computed tomography. *Curr. Biol. Mag.* **2017**, *27*, 283–293. [CrossRef] [PubMed]
18. Wei, Q.; Leblon, B.; La Rocque, A. On the use of X-ray computed tomography for determining wood properties: A review. *Can. J. For. Res.* **2011**, *41*, 11. [CrossRef]
19. Farinha, A.O.; Branco, M.; Pereira, M.F.C.; Auger-Rozenberg, M.; Maurício, A.; Yart, A.; Guerreiro, V.; Sousa, E.M.R.; Roques, A. Micro X-ray computed tomography suggests cooperative feeding among adult invasive bugs *Leptoglosus occidentalis* on mature seeds of stone pine Pinus pinea. *Agric. For. Entomol.* **2018**, *20*, 18–27. [CrossRef]
20. Fuchs, A.; Schreyer, A.; Feuerbach, S.; Korb, J. A new technique for termite monitoring using computer tomography and endoscopy. *Int. J. Pest Manag.* **2004**, *50*, 63–66. [CrossRef]
21. Himmi, S.K.; Yoshimura, T.; Yanase, Y.; Oya, M.; Torigoe, T.; Imazu, S. X-ray tomography analysis of the initial structure of the royal chamber and the nest-founding behaviour of the drywood termite Incisitermes minor. *J. Wood Sci.* **2014**, *60*, 453–460. [CrossRef]
22. Kigawa, R.; Torigoe, T.; Imazu, S.; Honda, M.; Harada, M.; Komine, Y.; Kawanobe, W. Detection of insects in wooden objects by X-ray CT scanner. *Sci. Conserv.* **2009**, *48*, 223–231. [CrossRef]
23. Watanabe, H.; Yanase, Y.; Fujii, Y. Evaluation of larval growth process and bamboo consumption of the bamboo powder-post beetle Dinoderus minutus using X-ray computed tomography. *J. Wood Sci.* **2015**, *61*, 171–177. [CrossRef]
24. Charles, F.; Coston-Guarini, J.; Guarini, J.; Lantoine, F. It's what's inside that counts: Computer-aided tomography for evaluating the rate and extent of wood consumption by shipworms. *J. Wood Sci.* **2018**, *64*, 427–435. [CrossRef]
25. ISO 13061-1:2014. *Physical and Mechanical Properties of Wood–Test Methods for Small Clear Wood Specimens–Part 1. Determination of Moisture Content for Physical and Mechanical Tests*; International Organization for Standardization: Geneva, Switzerland, 2014.

26. du Plessis, A.; Broeckhoven, C.; Guelpa, A.; Gerard le Roux, S. Laboratory x-ray micro-computed tomography: A user guideline for biological samples. *Gigascience* **2017**, *6*, 1–11. [CrossRef]
27. du Plessis, A.; Boshoff, W.P. A review of X-ray computed tomography of concrete and asphalt construction materials. *Constr. Build. Mater.* **2019**, *199*, 637–651. [CrossRef]
28. Singhal, A.; Grande, J.C.; Zhou, Z. Micro/nano CT for visualization of internal structures. *Microsc. Today* **2013**, *21*, 16–22. [CrossRef]
29. Campbell, G.M.; Sophocleous, A. Quantitative analysis of bone and soft issue by micro-computed tomography: Applications to ex vivo and in vivo studies. *BoneKEY Rep.* **2014**, *3*, 564. [CrossRef]
30. Maurício, A.; Figueiredo, C.; Alves, C.; Pereira, M.F.C.; Aires-Barros, L.; Neto, J.A.N. Non-destructive microtomography-based imaging and measuring laboratory-induced degradation of travertine, a random heterogeneous geomaterial used in urban heritage. *Environ. Earth Sci.* **2013**, *69*, 1471–1480. [CrossRef]
31. Ketcham, R.A.; Carlson, W.D. Acquisition, optimization and interpretation of X-ray computed tomography imagery: Applications to the geosciences. *Comput. Geosci.* **2001**, *27*, 381–400. [CrossRef]
32. Cnudde, V.; Cnudde, J.P.; Dupuis, C.; Jacobs, P.J.S. X-ray micro tomography used for the localisation of water repellents and consolidants inside natural building stones. *Mater. Charact.* **2004**, *53*, 259–271. [CrossRef]
33. Ketcham, R.A.; Iturrino, G.J. Nondestructive high-resolution visualization and measurement of anisotropic effective porosity in complex lithologies using high-resolution X-ray computed tomography. *J. Hydrol.* **2005**, *302*, 92–106. [CrossRef]
34. Rozenbaum, O.; Bergounioux, M.; Maurício, A.; Figueiredo, C.; Alves, C.; Barbanson, L. Versatile Three-Dimensional Denoising and Segmentation Method of X-ray Tomographic Images: Applications to Geomaterials Characterizations. Preprint 2016. Available online: https://hal.archives-ouvertes.fr/hal-01255507 (accessed on 13 April 2021).
35. Maurício, A.; Figueiredo, C.; Pereira, M.F.C.; Bergounioux, M.; Rozenbaum, O. Assessment of stone heritage decay by X-ray computed microtomography: II–a case of study of Portuguese limestones. *Microsc. Microanal.* **2015**, *21*, 162–163. [CrossRef]
36. Parkinson, I.H.; Badiei, A.; Fazzalari, N.L. Variation in segmentation of bone from micro-CT imaging: Implications for quantitative morphometric analysis. *Australas. Phys. Eng. Sci. Med.* **2008**, *31*, 160–164. [CrossRef]
37. Brozovsky, J.; Brozovsky, J.J.; Zach, J. An assessment of the condition of timber structures. In Proceedings of the 9th International Conference on NDT of Art, Jerusalem, Israel, 25–30 May 2008.